The diurnal evolution of 222Rn and its progeny in the atmospheric boundary layer during the Wangara experiment

J.-F. Vinuesa, S. Basu, S. Galmarini

Atmos. Chem. Phys. Discuss., 7, 8895–8931, 2007
www.atmos-chem-phys-discuss.net/7/8895/2007/

Atmospheric Chemistry and Physics Discussions

The diurnal evolution of ^{222}Rn and its progeny in the atmospheric boundary layer during the Wangara experiment

J.-F. Vinuesa[1], **S. Basu**[2], **and S. Galmarini**[1]

[1]European Commission – DG Joint Research Centre, Institute for Environment and Sustainability, 21020 Ispra, Italy
[2]Atmospheric Science Group – Department of Geosciences and Wind Science and Engineering Research Center, Texas Tech University, USA

Received: 10 May 2007 – Accepted: 11 June 2007 – Published: 25 June 2007

Correspondence to: J.-F. Vinuesa (jeff.vinuesa@jrc.it)

Abstract

The diurnal atmospheric boundary layer evolution of the ^{222}Rn decaying family is studied by using a state-of-the-art large-eddy simulation model. In particular, a diurnal cycle observed during the Wangara experiment is successfully simulated together with the effect of diurnal varying turbulent characteristics on radioactive compounds in a secular equilibrium. This study allows us to clearly analyze and identify the boundary layer processes driving the ^{222}Rn and its progeny concentration behaviors. The activity disequilibrium observed in the nocturnal boundary layer is due to the proximity of the radon source and the trapping of fresh ^{222}Rn close to the surface induced by the weak vertical transport. During the morning transition, the secular equilibrium is fast restored by the vigorous turbulent mixing. The evolution of ^{222}Rn and its progeny concentration in the unsteady growing convective boundary layer depends on the strength of entrainment events.

1 Introduction

The diurnal structure of the atmospheric boundary layer (ABL) has an important impact on the dispersion of chemical compounds. The main characteristic of the ABL is its turbulent nature that drives scalar transport with a broad range of spatial and temporal scales. Turbulent eddy motions transport and mix primary and secondary pollutants throughout the ABL. Large-scale turbulent eddy motions (e.g. thermals and subsidence motions) characterize the daytime convective boundary layer while the nocturnal boundary has significantly smaller eddies. In large-eddy simulation (LES), the largest eddies that are responsible for the turbulent transport of the scalars and momentum are explicitly solved whereas the smallest ones that are mainly dissipative are parameterized using a subgrid-scale (SGS) model. Since the seminal works by Deardorff (1970, 1972, 1974a,b, 1980), there have been numerous studies on LES of daytime buoyancy-driven boundary layers (Moeng and Wyngaard, 1984; Mason,

ACPD

7, 8895–8931, 2007

1989; Schumann, 1989; Sykes and Henn, 1989; Nieuwstadt et al., 1991; Khanna and Brasseur, 1997; Lewellen and Lewellen, 1998; Sullivan et al., 1998; Albertson et al., 1999), neutrally stratified ABL flows(Mason and Thomson, 1987; Andrén et al., 1994; Moeng and Sullivan, 1994; Lin et al., 1996; Kosović, 1997; Porté-Agel et al., 2000; Esau, 2004; Bou-Zeid et al., 2005; Chow et al., 2005; Stoll and Porté-Agel, 2006), and stably stratified ABL flows (Mason and Derbysire, 1990; Brown et al., 1994; Andrén, 1995; Saiki et al., 2000; Kosović and Curry, 2000; Basu and Porté-Agel, 2006; Beare et al., 2006). LES has enabled researchers to study various boundary layer flows by generating unprecedented high-resolution four-dimensional atmospheric turbulence data.

The full diurnal ABL cycle consists of the three flow regimes mentioned above and two transition states after sunrise and after sunset. The main limitation in simulating the diurnal ABL cycle resides in the difficulty of resolving both the small scales that characterize the nocturnal boundary layer and the large ones of the day time case with the same sub-grid scale model. A successful LES depends on the ability to accurately simulate the dynamics that are not explicitly resolved. The increasing atmospheric stability conditions from day to nighttime flow enhances the difficulty to perform successful simulations. A solution to the long standing issue of resolving the diurnal variation of the atmospheric boundary layer has recently been offered by the use of new generation scale-dependent dynamic subgrid-scale model (Kumar et al., 2006; Basu et al., 2007[1]). Both models are tuning-free, i.e. they do not require any ad-hoc specification of SGS coefficients. Kumar et al. (2006) used a Lagrangian approach (Bou-Zeid et al., 2005) that calculates the Smagorinsky coefficient dynamically at every position in the flow and as the flow evolves in time following fluid particle trajectories. Basu et al. (2007)[1] calculated both the Smagorinsky coefficient and the SGS Schmidt/Prandtl number using the locally-averaged scale-dependent dynamic (LASDD) SGS modeling approach (Basu and Porté-Agel, 2006; Basu et al., 2006). In addition, Basu et al. (2007)[1] have

[1]Basu, S., Vinuesa, J.-F., and Swift A.: Dynamic LES modeling of a diurnal cycle, J. Appl. Meteorol. Clim., in review, 2007.

demonstrated that the tuning-free LASDD SGS model based LES has the ability to capture the fundamental characteristics of observed atmospheric boundary layers even for very coarse resolutions.

Atmospheric dispersion of radon and its progeny has been of considerable interest since a number of years. ^{222}Rn is an unstable noble gas isotope of ^{226}Ra with a half-life of 3.8 days. Ground-based measurements and vertical distributions have been extensively studied to characterize the turbulent properties of the ABL, to perform regional and global circulation model benchmarking and to estimate regional surface fluxes of air pollutant and in particular climatically sensitive compounds. For instance, from one year measurements Galmarini (2006) once more demonstrated the ^{222}Rn ability of being an excellent tracer for boundary layer studies, Li and Chang (1996) used ^{222}Rn simulations to evaluate the modeled transport processes in a 3D global chemical transport model, Dentener et al. (1999) compared their model results with measurements to investigate the resolution sensitivity of their code, and Genthon and Armengaud (1995) or Jacob et al. (1997), among others, performed global atmospheric models evaluation and comparison using ^{222}Rn. In a recent study, Vinuesa and Galmarini (2007) used for the first time LES to characterize the turbulent transport of the ^{222}Rn and its progeny in academic ABLs. They simulated a steady-state convective ABL and ABL under unsteady conditions, e.g. representing the morning transition. They showed that the turbulent properties of the atmospheric convective boundary layers are of importance to study the dispersion and the transport of the ^{222}Rn family. In this present study, we broaden the recent work of Vinuesa and Galmarini (2007) by extending the study of the control exerted by turbulence on ^{222}Rn and its progeny atmospheric dispersion to the full range of stabilities characterizing atmospheric boundary layers. Not only we corroborate their findings for the unsteady convective boundary layer but we generalize and complete the study by simulating a realistic diurnal cycle consisting of the three stability regimes e.g. stable, neutral and unstable. In addition, by imposing secular equilibrium as initial condition, the issue of its possible disruption due to atmospheric stability can be addressed.

ACPD
7, 8895–8931, 2007

The paper is structured as follows. In Sect. 2, we describe the radioactive decay chain of ^{222}Rn. Simulation details of the observed case study are discussed in Sect. 3. In Sect. 4, general results on the diurnal dispersion of ^{222}Rn and its progeny are presented. These results are detailed in the three following sections by focusing on the dispersion during the night, the daytime turbulent dispersion and the evolution of the mixed-layer quantities. Section 8 is devoted to the disruption of the secular equilibrium due to the atmospheric stability and an analysis of the disequilibrium activity ratios of ^{222}Rn and its short-lived daughters is provided. Finally, concluding remarks are drawn in Sect. 9.

2 ^{222}Rn decaying chain and turbulent dispersion

We consider the radioactive decay chain of ^{222}Rn that reads:

$$^{222}\mathrm{Rn} \xrightarrow{\lambda_{^{222}\mathrm{Rn}}} {}^{218}\mathrm{Po} \xrightarrow{\lambda_{^{218}\mathrm{Po}}} {}^{214}\mathrm{Pb} \xrightarrow{\lambda_{^{214}\mathrm{Pb}}} {}^{214}\mathrm{Bi} \xrightarrow{\lambda_{^{214}\mathrm{Bi}}} {}^{210}\mathrm{Pb}, \quad (1)$$

where $\lambda^{^{222}\mathrm{Rn}}$, $\lambda^{^{218}\mathrm{Po}}$, $\lambda^{^{214}\mathrm{Pb}}$ and $\lambda^{^{214}\mathrm{Bi}}$ are the decay frequencies equal to 2.11×10^{-6}, 3.80×10^{-3}, 4.31×10^{-4}, and $5.08\times10^{-4}\mathrm{s}^{-1}$, respectively. Note that we consider a direct transformation of ^{214}Bi into ^{210}Pb since the half-life of ^{214}Po (daughter of ^{214}Bi) is very short (164µs). Also we consider ^{210}Pb, that has a half-life of 22.3 years, as an inert scalar with respect to the temporal scales considered here. To increase readability, ^{222}Rn and its progeny activity (number of atoms) concentrations will be also referred to as S_i (n_i) where i is the rank of the daughter in the decay chain (e.g. 0 stands for ^{222}Rn and 4 for ^{210}Pb). In large-eddy simulation, the filtered conservation equation for a radioactive scalar involved in a chain of reactions is

$$\frac{\partial \widetilde{n}_i}{\partial t} + \widetilde{u}_j \frac{\partial \widetilde{n}_i}{\partial x_j} = -\frac{\partial Q_{i,j}}{\partial x_j} + \widetilde{R}_i \quad (2)$$

ACPD
7, 8895–8931, 2007

where $\widetilde{n_i}$ is the spatially filtered (at scale Δ) scalar concentration n_i, $\widetilde{R_i}$ is its radioactive source/sink term and $Q_{i,j}$ is its subgrid-scale (SGS) flux defined as:

$$Q_{i,j} = \widetilde{u_j n_i} - \widetilde{u}_j \widetilde{n}_i, \tag{3}$$

For the chain (1), the $\widetilde{R_i}$ read:

$$\widetilde{R_0} = -\lambda_0 \widetilde{n_0}, \tag{4}$$

$$\widetilde{R_1} = \lambda_0 \widetilde{n_0} - \lambda_1 \widetilde{n_1}, \tag{5}$$

$$\widetilde{R_2} = \lambda_1 \widetilde{n_1} - \lambda_2 \widetilde{n_2}, \tag{6}$$

$$\widetilde{R_3} = \lambda_2 \widetilde{n_2} - \lambda_3 \widetilde{n_3}, \tag{7}$$

$$\widetilde{R_4} = \lambda_3 \widetilde{n_3}. \tag{8}$$

As one can see, the process is unidirectional with the concentration of ^{222}Rn initial concentration flowing from daughter to daughter. In such condition, the expected effect of turbulence will relate to the mixing of the different species. One could expect that species produced (decaying) faster than others may appear (disappear) in (from) specific regions of the ABL as due to the turbulent transport and mixing process. The timescale of the turbulent transport and how it relates to the timescale of the radioactive decay is one of the governing parameters of the process. The deviation from the secular equilibrium is often used as an indicator of the residence time in the atmosphere or as an indicator of the atmospheric stability. The secular equilibrium is the condition according to which the ratio of the activities of the nuclide participating to the decay chain is equal to 1, namely:

$$\frac{\lambda_{i+1} \widetilde{n_{i+1}}}{\lambda_i \widetilde{n}_i} = 1 \tag{9}$$

This corresponds to a balance between production and destruction of the nuclide. One of the foci of this study is to determine whether an initial condition of secular equilibrium

ACPD
7, 8895–8931, 2007

is disrupted during the full daily evolution of the ABL and given a constant in-flux of ^{222}Rn at the surface as due to the simultaneous occurrence of mixing and radioactive decay.

3 Description of the simulation

In this work, the simulation is performed with a modified version of 3-dimensional LES code described by Albertson et al. (1999); Porté-Agel et al. (2000); Porté-Agel (2004) in which a chemical solver has been recently introduced (Vinuesa and Porté-Agel, 2005). We use the newly proposed "locally-averaged scale-dependent dynamic" (LASDD) SGS modeling approach (Basu and Porté-Agel, 2006; Basu et al., 2006) for simulations of an diurnal cycle observed during Wangara experiment. The LASDD SGS model is completely tuning-free in contrast to most of the conventional eddy-viscosity and eddy-diffusivity SGS models. In other words, the LASDD SGS model does not require any ad-hoc specification of SGS coefficients, since they are computed dynamically based on the local dynamics of the resolved velocity and temperature fields in a self-consistent manner. The Wangara experiment was conducted during July and August 1967 at Hay in Australia (Clarke et al., 1971; Hess et al., 1981). Basu et al. (2007)[1] presented the first LES study of a diurnally varying ABL observed during the Wangara case study. Their simulation were performed for a full diurnal cycle, from 09:00 LST, day 33 (16 August 1967) to 09:00 LST, day 34 (17 August 1967). In the present study, we are also interested in the interaction between the ABL and the reservoir layer above it, we extend the simulation up to 18:00 LST of day 34. Since the initialization of the simulation, the surface and large-scale forcing are fully detailed in Basu et al. (2007)[1], we only give here a brief summary.

The LES model is initialized with 09:00 LST sounding of day 33. The lower boundary condition is based on the Monin-Obukhov similarity theory with a surface roughness length z_o=0.01 m. Following Yamada and Mellor (1975), the screen temperature at 1.2 m is used for sensible heat flux estimation and vertical profiles of geostrophic wind

components (U_g, V_g) at any instant are calculated by fitting parabolic profiles to the observed surface geostrophic wind and thermal wind values. Finally, these values are linearly interpolated between the observation times (see Yamada and Mellor (1975) for further details). The Coriolis parameter is set to $f_c = -0.826 \times 10^{-4}$ s^{-1} corresponding to latitude 34°30′ S. Following previous studies (e.g., Jacobi and Andre, 1963; Beck and Gogolak, 1979), the exhalation rate of radon is set at typical value of 1.0 atom cm^{-2} s^{-1}. A secular equilibrium between radon and its progeny is imposed as initial condition. The selected domain size is 5000 m×5000 m×2000 m. In Basu et al. (2007)[1], this domain was divided into: 160×160×160 grid-points. However, Basu and Porté-Agel (2006) found that the LASDD model simulated statistics are quite insensitive to grid resolution. This was confirmed by Basu et al. (2007)[1] that showed that even with a coarse resolution of 80×80×80 grid points, the LASDD SGS model is able to capture the essential characteristics of the observed nighttime boundary layer (e.g. the magnitude, timing and location of the low-level jet wind maxima). Thus, we choose this latter resolution for the present study since the CPU demand and space requirement are enhanced by the addition of the radioactive decaying chain in the simulation. This leads to a grid resolution of 62.5 m×62.5 m×25.0 m. Periodic lateral boundary conditions are assumed and the time step is set to 1 s.

The results relative to the wind and the potential temperature are briefly summarized in the following, see Basu et al. (2007)[1] for a complete analysis. Figure 1 shows the observed and simulated longitudinal and lateral components of velocity. During daytime, as a result of turbulent mixing, the wind profiles were observed to be nearly constant in the mixed layer. During night 33–34, a low-level jet (LLJ) developed due to inertial oscillation. Initially, the magnitude of the LLJ wind maxima increased with time (till approximately 03:00 LST) and then decreased. The observed LLJ height was approximately 200 m. From this figure, it is clear that our LES model has successfully captured the development, magnitude and location of the observed LLJ. The evolution of simulated mean temperatures is compared with observations in Fig. 2. Thin, very unstable surface layer, and mixed layer topped by a stable inversion layer are discernible during

the two daytimes. At nighttime, strong surface based inversion develops as would be expected. These features are qualitatively well reproduced by the LES model.

4 Diurnal evolution of ^{222}Rn and its progeny concentrations as if ^{222}Rn was emitted during the Wangara experiment

In the following sections, we focus our analysis on the 24-h diurnal cycle starting at 18:00 LST on day 33. The part of the simulation chosen to perform our analysis corresponds to a situation with realistic concentration profiles of ^{222}Rn and its progeny in the reservoir layer. Thus the beginning of the simulation, i.e. from 09:00 LST to 18:00 LST of day 33 allowed us to reproduce a realistic distribution of the nuclide in the atmosphere and then reduce the inherent forcing due to an imposed uniform initial distributions. In other terms, this period can be considered as a spin-up period of the simulation that allows a realistic spatial distribution consistent with boundary-layer mixing processes and secular equilibrium. In this section, the overall diurnal cycle is analyzed whereas the next two will focus on the specific processes responsible for the dispersion during the night and the day. Figure 3 shows the time evolution of the concentration of the mother ^{222}Rn (S_0) and its progeny. Around sunset, vertical motions are suppressed due to the cooling at the surface. This cooling results in a temperature stable stratification and in the formation of a thin boundary layer isolating the surface from the upper atmosphere layer. In this layer, turbulence decays, leaving a residual layer in place of the well-mixed convective layer. The nocturnal BL is characterized by very high concentrations and important concentration vertical gradients. Over the night, S_0 is emitted constantly and, due to the stability of the NBL, it is accumulating close to the surface. S_0 and its short-lived daughters undergo the unidirectional chain of reactions with the radon concentration flowing into the daughter's. As a result, S_0 progeny also accumulates close to the surface.

At sunrise, the solar heating causes thermal plumes to rise. These plumes expand up to the top of the atmospheric boundary layer where a thermodynamic equilibrium is

reached. Air from the free atmosphere penetrates down, replacing rising air parcels. Narrow vigorous thermals surrounded by relatively large subsidence motions generate turbulent mixing leading to a so-called mixed layer where, for instance, potential temperature is nearly constant with height. During the morning transition and the development of the unstable boundary layer, we find results similar to Vinuesa and Galmarini (2007). The concentration of all radio nuclei reduces abruptly in spite of the fresh emission of S_0. These concentrations are driven by the production through the decaying chain, the dilution due to boundary layer deepening and the entrainment of lower concentration air masses from the reservoir layers. Under unstable conditions, dilution is driving the concentration behavior. The reservoir layer is decoupled from the surface during nighttime due to the stable stratification of the nocturnal boundary layer and during daytime due to the capping inversion at the top of the convective boundary layer. No fresh emissions of S_0 can reach the reservoir layer and the radionuclide concentrations are decreasing with time.

The time evolution of the concentrations is the result of the combined effect of the divergence of the fluxes and the radioactive decay contribution. In order to understand which process is responsible for the ^{222}Rn and its short-lived daughters activity behavior, we will focus on the fluxes and the radioactive decay contributions in the next two sections. For the daytime period, one will notice that we found similar results as Vinuesa and Galmarini (2007) in their academic unsteady CBL simulation. Actually the present findings extend and corroborate their results to a full diurnal cycle, a realistic planetary boundary layer and a radon decaying family in or close to the secular equilibrium.

5 Dispersion during the night

In this section, we focus on the nighttime dispersion of radon and its progeny and we analyze the results for the stable nocturnal period from 18:00 LST on day 33 to 08:00 LST on day 34. The evolution of the sensible surface heat flux dynamically

calculated from prescribed screen temperature at 1.2 m and temperature at first LES model level is shown in Fig. 4. As a result, the cooling at the surface occurs from 17:30 LST to 08:30 LST. The nocturnal boundary layer depth is ranging from 100 to 500 m and we will focus on this part of the atmosphere. The low level stratification of the nocturnal boundary layer induces the accumulation of freshly emitted S_0 close to the surface (Fig. 5). In this area, the proportion of freshly emitted radon is higher than above. This layer can be considered as a "fresh radon layer" and since radon is slowly decaying, the amount of freshly created daughters is smaller than in upper regions. As a result, the presence of the "fresh radon layer" induces a rapid departure from secular equilibrium. The disequilibrium prevails during the night since fresh radon is constantly injected at the surface. As a result, S_0 concentrations show an almost linear increase whereas the build up of the daughters' concentrations is slower and delayed. The weak vertical mixing is responsible for the accumulation of radon and its progeny close to the surface. The important temporal variability of the fluxes suggests that vertical transport events are very localized in space and time (Fig. 6). One can note that while the maximum vertical flux of radon are located close to the surface, the maximum flux location is moving upwards while the rank of the daughter in the ^{222}Rn progeny is increasing. Since all daughters are produced by the radioactive decomposition of S_0 and only a weak vertical transport is found in the NBL, one would expect to find maximum daughter fluxes close to the surface. Actually, these maximum fluxes are found in places where the vertical concentration gradients are stronger. In comparison, a similar vertical distribution of the radioactive decay contributions is not found (Fig. 7). For these later contributions, the maximum is found close to the surface.

Figure 7 reveals strong vertical gradients of radioactive decay contributions to the short-lived daughters concentrations. These gradients are related to the concentration imbalance between the members of radon decaying family. Since ^{218}Po (S_1) is the first daughter of the family, its production by the decay of S_0 is more important where the S_0 concentrations are higher, i.e. close to the surface. Its radioactive decay proceeds at a faster rate than the mixing. Since mixing is very weak in the NBL, freshly created

ACPD
7, 8895–8931, 2007

^{218}Po is decaying before being transported. As a result, its radioactive contribution is mostly acting close to the surface. The same process occurs for R_2 and R_3 even if due their slower decaying rates of (S_2) and (S_3), the vertical gradients are not as strong as the ones of R_1.

6 Daytime turbulent dispersion

Figure 8 shows the time evolution of the concentration of ^{222}Rn (S_0) and the short-lived daughters S_1, S_2 and S_3. No fresh emissions of S_0 reach the reservoir layer resulting from the previous day CBL and from the nocturnal BL since they are decoupled from the surface. Radon and its progeny concentrations decrease with time in the reservoir layer as result of the decaying process. The same boundary layer concentration behaviors can be observed for S_0 and the daughters; as the boundary layer deepens with time, the concentrations decrease despite of fresh emission of radon and the production of the daughters through the decay chain. As mentioned previously, these concentrations are the result of antagonist effects: the production by the decaying chain, the dilution by boundary layer deepening and the ventilation due to the entrainment of lower concentration air masses from the reservoir layer. In order to understand which process is responsible for the collapse of the ^{222}Rn and its short-lived daughters concentration during the morning transition of the convective boundary layer, we focus in the following on the vertical profiles of the fluxes (Fig. 9) and the radioactive decay contributions (Fig. 10). The growth of the boundary layer is inducing ventilation at the top of the CBL. While the boundary layer is deepening, air masses with smaller concentrations are entrained from above. Turbulence transport is locally balancing the gradient of concentration induced by the entrainment of cleaner air by transporting radionuclide toward the upper boundary layer. This upward flux is more vigorous when the ventilation process is enhanced by the increase of the boundary layer growth rate. As a result we found important detrainment fluxes, e.g. positive flux values at the entrainment, even more important than the emission flux for S_0. Actually,

two detrainment flux maxima can be noted when looking closely to the figure: one at 10:00 LST and the one at around 12:30 LST. These maxima occur when the growth of the boundary layer depth shows a maximum and so does the entrainment velocity w_e (see Fig. 11). This confirms that the high flux values are due to the entrainment of low concentration air masses from above the CBL.

The radioactive decay term acts as a sink for S_0 and as a source for its progeny. All contributions show a maximum close to the surface together with different vertical gradients: the one of R_1 is extreme compared to the ones of R_2 and R_3. This latter shows an almost well-mixed profile in the lower-CBL. However, a maximum contribution at the bottom of the entrainment layer can be noticed. This behavior was already mentioned by Vinuesa and Galmarini (2007) that attributed it to the inability of turbulence to mix efficiently radon short-lived daughters that have a decaying temporal scale comparable to the turnover time of the CBL. Our findings confirm their analysis for a more realistic simulation.

7 Focusing on the mixed-layer characteristics

Figure 11 shows the evolution of the convective boundary layer growth focusing on the boundary layer depth z_i defined as the height where the minimum sensible heat flux is found, the entrainment velocity w_e that is the speed of the boundary layer growth, i.e. $\frac{dz_i}{dt}$ and the ratio of entrainment to the surface flux of potential temperature β_θ. From this figure, three periods can be distinguished related to the characteristics of the unsteady growth of the CBL. After sunrise, the convective boundary layer starts to develop overlayed by the stable nocturnal boundary layer. At the top of it, the strong capping inversion is preventing thermals to develop. As a result, the boundary layer growth is slow but increasing as the CBL deepens. At around 10:00 LST, the boundary layer top reaches the maximum extension of the previous nocturnal boundary layer. Due to the increase of the capping inversion at this interfacial layer (between the residual of the previous nocturnal boundary layer and the previous day convective boundary

ACPD
7, 8895–8931, 2007

layer) the growth is slow down. Then the boundary layer continues to develop but now overlayed by the residual layer of the previous day CBL. The temperature jump at the top of the CBL is lower than previously (see also Fig. 1) and the growth is enhanced due to small temperature gradients across the entrainment zone. The boundary layer doubles its vertical extension within a few hours. At around 12:30 LST, the top of the CBL reaches the free troposphere. The strong capping inversion limits its development, the entrainment velocity dramatically collapse and the CBL depth is evolving toward a steady-state. The sharpness of the peak of entrainment velocity located at around 12:30 LST reflects the strength of the inversion. Actually these periods are much more distinguishable while focusing on the mixed-layer concentrations of ^{222}Rn and its progeny i.e. $\langle S_i \rangle$ and the ratio of entrainment to the surface flux of ^{222}Rn $\beta_0 = \frac{-(\overline{ws_0})_e}{(\overline{ws_0})_s}$ where $(\overline{ws_0})_e$ and $(\overline{ws_0})_s$ are the entrainment and surface flux of S_0, respectively. The $\langle S_i \rangle$ and β_0 are shown in Fig. 12

- To 09:30 LST: Initialization of convection, a sharp mixed-layer starts to develop overlayed by a strong stratification.
- From 09:30 to 10:00 LST: The mixed-layer is developing within the leftover of the stable nocturnal boundary layer. $\langle S_i \rangle$ decrease due to the entrainment of less radon-concentrated air masses at the top of the CBL. This decrease is limited since air masses above the mixed layer contains S_i that has been trapped during the night.
- From 10:00 to 11:30 LST: The mixed-layer is developing overlayed by the residual layer and $\langle S_i \rangle$ collapse. During the night, the reservoir layer has been almost decoupled from the surface due to the stable stratification of the nocturnal boundary layer. Since no fresh radon reached this layer, the radon short-lived daughter mixture aged and the system evolved toward secular equilibrium. S_i is less abundant is the reservoir layer than in the leftover of nocturnal boundary layer. Therefore, ventilation is entraining cleaner radon air masses than during the previous period

ACPD
7, 8895–8931, 2007

and the decrease of $\langle S_i \rangle$ is more important.

– From 11:30 LST: The mixed-layer top has reached the free troposphere. The ventilation process still occurs but it is less important due to the collapse of w_e and the low concentration gradient at the entrainment. The retrieval of the mixed-layer secular equilibrium is facilitated by the entrainment of radon and daughters mixture already in equilibrium.

8 Secular equilibrium

If the radon daughters were subject only to the laws of radioactive decay, the secular equilibrium imposed in the initial activity profiles would be conserved along the simulation. However, departures from the equilibrium can be noticed in Fig. 13 that shows the radon and its short-lived daughters activity ratios. This disequilibrium is more important under stable stratification in the nocturnal boundary layer. Under convective conditions, the ratios evolve toward the equilibrium value of one that is retrieved after the morning transition. At the end of the day, the surface cooling results in a temperature stable stratification and in the formation of a thin boundary layer isolating the surface from the upper atmosphere layer. In this layer, turbulence decays and departures from the equilibrium occur. It is interesting to notice that the equilibrium reached in the mixed layer of the previous day is preserved in the reservoir layer. There has been extensive measurements of the disequilibrium ratios in the surface layer for various type of stabilities (e.g. Beck and Gogolak, 1979; Hosler and Lockhart, 1965; Hosler, 1966). The largest departures from the secular equilibrium were reported under stable conditions. The disequilibrium ratio was found to be also dependent on both the distance from the surface and the duration of the stability regime. Quite a number of one-dimensional models have been formulated to relate the vertical distribution of the radionuclide to the eddy diffusivity and to the exhalation rate of radon (e.g. Jacobi and Andre, 1963; Staley, 1966) and reached the same conclusions.

Several studies in the past have tried to correlate the stability regime with S_0 or the disequilibrium activity ratio. However, even if at first glance it appears that the equilibrium levels might be correlated directly with stability regime in the surface layer, the results shown in Fig. 14 reveal that other boundary layer characteristics should be considered. A given air parcel can be considered as a mixture of radon and its short-lived daughters. At sunset, if this parcel is close to the emission source of radon, it is composed of more freshly emitted radon than "old" radon. Because of the slow decay of radon, this air parcel contains more radon than its short-lived daughters. As a result, radon and its short-lived daughters activity ratios are lower than 1. Throughout the night, the proportion of aging radon is increasing (compared to "fresh" radon) and the mixture is evolving toward equilibrium. However, since the radioactive half-life of ^{222}Rn is 3.8 days, the night is obviously not long enough to enable the secular equilibrium to be restored. In Fig. 14, one can notice that the activity ratios collapse in the evening and increase during the night.

During the convective daytime period, turbulent eddy motions are mixing the radon being exhaled from the soil into aged radon mixture. Due to the mixing and the short turnover time, any air parcel of the CBL contains the same amount of "fresh" radon and "old" radon. Turbulent transport enables the radioactive system to evolve toward the equilibrium. As a result, after the morning transition the equilibrium is reached and the homogeneous composition of the radon and short-lived daughter mixture is maintained by the turnover of the CBL. Figure 14 shows important increases of the activity ratio during the morning transition. Most of all, our results shows that the activity ratio between radon and its progeny cannot be used solely as an indicator of atmospheric stability for diurnal evolving ABL. As one can clearly see in Fig. 14 two values of the ratio correspond to the same stability value. In this figure, one can notice importance differences in the departure from secular equilibrium at dusk for the equilibrium ratios. During the initiation of the stable nocturnal boundary layer, the change of S_1/S_0 activity ratio is rather small while the one of S_3/S_0 can reach 4%. One may wonder if these differences can be explained in term of mixing by nocturnal turbulence. An appropri-

ate number to investigate the effect of turbulence on the radionuclei is the Damköhler number (Vinuesa and Galmarini, 2007). In Fig. 15, the Damköhler numbers Da_t for Radon and its short-lived daughters are plotted against Obhukov length. The Da_t can be defined as the ratio between the integral time-scale of turbulent (τ_t) and the chemical time-scale (τ_c). $\tau_t = z_i / w_*$ for the convective boundary layer and $\tau_t = h/u_*$ for the nocturnal one. z_i and h are defined as the altitude where the sensible heat flux is minimum and where the turbulent heat flux is 5% of its surface value (Estournel and Guedalia, 1985), respectively. For the radionuclides, $\tau_c = \lambda_j^{-1}$ with j=0, 1, 2, 3 meaning that the Damköhler numbers differ by the radioactive decaying rates. Therefore S_1 and S_2 should be the most and the less affected daughters, respectively. However, the most important departure for secular equilibrium is found for S_3. This clearly shows that nocturnal turbulence do not have an impact on the departure from secular equilibrium at dusk and, as mentioned previously, the driving process is the aging of the mixture of radon and short-lived daughters.

9 Conclusions

Numerical experiments were carried out using the state-of-the-art large-eddy simulation together with a new-generation subgrid-scale model to study the diurnal evolution of ^{222}Rn and its progeny in the atmospheric boundary layer. An observed diurnal cycle was successfully simulated and for the first time, the simulation included first-order decaying system represented by the the decaying chain of the ^{222}Rn family. By focusing our analysis on the night 33–34 and day 34 of the Wangara experiment, e.g. using the simulation of day 33 as a pre-run, and initializing the ^{222}Rn and short-lived daughters' concentrations as in a secular equilibrium, we were able to reproduce the realistic diurnal evolution of the ^{222}Rn decaying family. Near the surface, radon concentrations increase during the nocturnal stable period, reaching a maximum near sunrise. Following the breakup of a nocturnal surface-based radiation-type inversion, radon concentrations decrease rapidly, reaching a minimum during the afternoon convective period.

ACPD
7, 8895–8931, 2007

A departure from secular equilibrium between radon and its short-lived daughter products prevails in the stable nocturnal boundary layer. This disequilibrium is attributed to the proximity of the radon source and the weak vertical transport. Since a significant fraction of the radon is fresh, the radon and progeny mixture is deficient in daughters. The mixing induced by convective turbulence induces a fast restoration of the secular equilibrium during the morning transition. Both turbulent transport and transport asymmetry of ^{222}Rn daily evolution confirm that the ventilation at the entrainment zone induced by the unsteady growth of the boundary layer entrains cleaner air from the leftover of the residual layers, e.g. the residual nocturnal boundary layer and the reservoir layer resulting from the previous day boundary layer. These entrainment events are responsible for the collapse of the mixed layer concentrations. The analysis of the different contributions to the evolution of concentrations reveals that the spatial and temporal evolution of the concentrations is directly related to radioactive decay contribution in which turbulent mixing plays the major role. Thus, turbulent transport affect the dispersion of ^{222}Rn and its progeny by acting preferentially on the radioactive decay.

Acknowledgements. Computational resources were kindly provided by the High Performance Computing Center at the Texas Tech University.

References

Albertson, J. D. and Parlange, M. B.: Natural integration of scalar fluxes from complex terrain, Adv. Wat. Res., 23, 239–252, 1999. 8897, 8901

Andrén, A., Brown, A. R., Graf, J., Mason, P. J., Moeng, C.-H., Nieuwstadt, F. T. M., and Schumann, U.: Large-eddy simulation of a neutrally stratified boundary layer: A comparison of four computer codes, Quart. J. Roy. Meteorol. Soc., 120, 1457–1484, 1994. 8897

Andrén, A.: The structure of stably stratified atmospheric boundary layers: a large-eddy simulation study, Quart. J. Roy. Meteorol. Soc., 121, 961–985, 1995. 8897

Basu, S. and Porté-Agel, F.: Large-eddy simulation of stably stratified atmospheric boundary

layer turbulence: a scale-dependent dynamic modeling approach, J. Atmos. Sci., 63, 2074–2091, 2006. 8897, 8901, 8902

Basu, S., Porté-Agel, F., Foufoula-Georgiou, E., Vinuesa, J.-F., and Pahlow, M.: Revisiting the local scaling hypothesis in stably stratified atmospheric boundary-layer turbulence: an integration of field and laboratory measurements with large-eddy simulations, Boundary-Layer Meteorol., 119, 473–500, 2006. 8897, 8901

Beare, R. J., Macvean, M. K., Holtslag, A. A. M., Cuxart, J., Esau, I., Golaz, J.-C., Jimenez, M. A., Khairoutdinov, M., Kosovic, B, Lewellen, D., Lund, T. S., Lundquist, J. K., Mccabe, A., Moene, A. F., Noh, Y., Raasch, S., and Sullivan, P.: An intercomparison of large-eddy simulations of the stable boundary layer, Boundary-Layer Meteorol., 118, 247–272, 2006. 8897

Beck, H. L. and Gogolak, C. V.: Time dependent calculation of the vertical distribution of 222Rn and its decay products in the atmosphere, J. Geophys. Res., 84, 3139–3148, 1979. 8902, 8909

Bou-Zeid, E., Meneveau, C., and Parlange, M.: A scale-dependent Lagrangian dynamic model for large eddy simulation of complex turbulent flows, Phys. Fluids, 17, 025105, 2005. 8897

Brown, A. R., Derbyshire, S. H., and Mason, P. J.: Large-eddy simulation of stable atmospheric boundary layers with a revised stochastic subgrid model, Quart. J. Roy. Meteorol. Soc., 120, 1485–1512, 1994. 8897

Chow, F. K., Street, R. L., Xue, M., and Ferziger, J. H.: Explicit filtering and reconstruction turbulence modeling for large-eddy simulation of neutral boundary layer flow, J. Atmos. Sci., 62, 2058–2077, 2005. 8897

Clarke, R. H., Dyer, A. J., Brook, R. R., Reid, D. G., and Troup, A. J.: The Wangara experiment: boundary layer data, Paper No. 19, Div. of Meteorol. Physics Aspendale, CSIRO, Australia, 362pp., 1971. 8901

Deardorff, J. W.: Preliminary results from numerical integrations of the unstable planetary boundary layer, J. Atmos. Sci., 27, 1209–1211, 1970. 8896

Deardorff, J. W.: Numerical investigation of neutral and unstable planetary boundary layers, J. Atmos. Sci., 29, 91–115, 1972. 8896

Deardorff, J. W.: Three-dimensional numerical study of the height and mean structure of a heated planetary boundary layer, Boundary-Layer Meteorol., 7, 81–106, 1974a. 8896

Deardorff, J. W.: Three-dimensional numerical study of turbulence in an entraining mixed layer, Boundary-Layer Meteorol., 7, 199–226, 1974b. 8896

Deardorff, J. W.: Stratocumulus-capped mixed layers derived from a three-dimensional model, Boundary-Layer Meteorol., 18, 495–527, 1980. 8896
Dentener, F., Feichter, J., and Jeuken, A.: Simulation of the transport of Rn-222 using on-line and off-line global models at different horizontal resolutions: a detailed comparison with measurements, Tellus, 51B, 573–602, 1999. 8898
Esau, I.: Simulation of Ekman boundary layers by large eddy model with dynamic mixed subfilter closure, Environ. Fluid Mech., 4, 273–303, 2004. 8897
Estournel, C. and Guedalia, D: Influence of geostrophic wind on atmospheric nocturnal cooling, J. Atmos. Sci., 42, 2695–2698, 1985. 8911, 8921, 8922, 8923
Galmarini, S.: One year of 222-Rn concentration in the atmospheric surface layer, Atmos. Chem. Phys. 6, 2865–2887, 2006. 8898
Genthon, C. and Armengaud, A.: Radon-222 as a comparative tracer of transport and mixing in 2 general-circulation models of the atmosphere, J. Geophys. Res., 100, 2849–2866, 1995. 8898
Hess, G. D., Hicks, B. B., and Yamada, T.: The impact of the Wangara experiment, Boundary-Layer Meteorol., 20, 135–174, 1981. 8901
Hosler, C. R. and Lockhart, L. B.: Simultaneous measurment of ^{222}Rn, ^{214}Pb and ^{214}Bi in air near the ground, J. Geophys. Res., 70, 4537–4546, 1965. 8909
Hosler, C. R.: Meteorological effects on atmospheric concentrations of Radon (Rn^{222}), RaB (Pb^{214}), and RaC (Bi^{214}) near the ground, Mon. Wea. Rev., 94, 89–99, 1966. 8909
Jacob, D. J., Prather, M. J., Rasch, P. J., Shia, R. L., Balkanski, Y. J., Beagley, S. R., Bergmann, D. J., Blackshear, W. T., Brown, M., Chiba, M., Chipperfield, M. P., deGrandpre, J., Dignon, J. E., Feichter, J., Genthon, C., Grose, W. L., Kasibhatla, P. S., Kohler, I., Kritz, M. A., Law, K., Penner, J. E., Ramonet, M., Reeves, C. E., Rotman, D. A., Stockwell, D. Z., VanVelthoven, P. F. J., Verver, G., Wild, O., Yang, H., and Zimmermann, P.: Evaluation and intercomparison of global atmospheric transport models using Rn-222 and other short-lived tracers, J. Geophys. Res., 102, 5953–5970, 1997. 8898
Jacobi, W. and Andre, K.: The vertical distribution of ^{222}Rn, ^{220}Rn and their decay products in the atmosphere, J. Geophys. Res., 68, 3799–3814, 1963. 8902, 8909
Khanna, S. and Brasseur, J. G.: Analysis of Monin-Obukhov similarity from large-eddy simulation, J. Fluid Mech., 345, 251–286, 1997. 8897
Kumar, V., Kleissl, J., Meneveau, C., and Parlange, M. B.: Large-eddy simulation of a diurnal cycle of the atmospheric boundary layer: Atmospheric stability and scaling issues, Water

Resour. Res., 42, W06D09, doi:10.1029/2005WR004651, 2006. 8897
Kosović, B.: Subgrid-scale modelling for the large-eddy simulation of high-Reynolds-number boundary layers, J. Fluid Mech., 338, 151–182, 1997. 8897
Kosović, B. and Curry, J. A.: A large eddy simulation study of a quasi-steady, stably stratified atmospheric boundary layer, J. Atmos. Sci., 57, 1052–1068, 2000. 8897
Lewellen, D. C. and Lewellen, W. S.: Large-eddy boundary layer entrainment, J. Atmos. Sci., 55, 2645–2665, 1998. 8897
Li, Y. H. and Chang, J. S.: A three-dimensional global episodic tracer transport model. 1. Evaluation of its processes by radon 222 simulations, J. Geophys. Res., 101, 25 931–25 947, 1996. 8898
Lin, C.-L., McWilliams, J. C., Moeng, C.-H., and Sullivan, P. P.: Coherent structures and dynamics in a neutrally stratified planetary boundary layer flow, Phys. Fluids, 8, 2626–2639, 1996. 8897
Mason, P. J. and Thomson, D. J.: Large-eddy simulations of the neutral-static-stability planetary boundary layer, Quart J. Roy. Meteorol. Soc., 113, 413–443, 1987. 8897
Mason, P. J.: Large-eddy Simulation of the Convective Atmospheric Boundary Layer, J. Atmos. Sci., 46, 1492–1516, 1989. 8896
Mason, P. J. and Derbysire, S. H.: Large-eddy simulation of the stably-stratified atmospheric boundary layer, Boundary-Layer Meteorol., 53, 117–162, 1990. 8897
Moeng, C. H. and Wyngaard, J. C.: Statistics of conservative scalars in the convective boundary layer, J. Atmos. Sci., 41, 3161–3169, 1984. 8896
Moeng, C. H. and Sullivan, P. P.: A comparison of shear- and buoyancy-driven planetary boundary layer flows, J. Atmos. Sci., 51, 999–1022, 1994. 8897
Nieuwstadt, F. T. M., Mason, P. J., Moeng, C.-H., and Schumann, U.: Large-eddy simulation of the convective boundary layer: a comparison of four computer codes, in: Turbulent Shear Flows 8, edited by: Durst, F. , Friedrich, R., Launder, B. E., Schmidt, F. W., Schumann, U., and Whitelaw, J. H., Springer, 347–367, 1991. 8897
Porté-Agel, F., Meneveau, C., and Parlange, M. B.: A scale-dependent dynamic model for large-eddy simulations: application to a neutral atmospheric boundary layer, J. Fluid Mech., 415 , 261–284, 2000. 8897, 8901
Porté-Agel, F.: A scale dependent dynamic model for scalar transport in LES of the atmospheric boundary layer, Boundary-Layer Meteorol., 112, 81–105, 2004. 8901
Saiki, E. M., Moeng, C.-H., and Sullivan, P. P.: Large-eddy simulation of the stably stratified

planetary boundary layer, Boundary-Layer Meteorol., 95, 1–30, 2000. 8897
Schumann, U.: Large-eddy simulation of turbulent diffusion with chemical reactions in the convective boundary layer, Atmos. Environ., 23, 1713–1729, 1989. 8897
Staley, D. O.: The diurnal oscillations of radon and thoron and their decay products, J. Geophys. Res., 71, 3357–3367, 1966. 8909
Stoll, R. and Porté-Agel, F.: Dynamic subgrid-scale models for momentum and scalar fluxes in large-eddy simulations of neutrally stratified atmospheric boundary layers over heterogeneous terrain, Water. Resour. Res., 42, W01409, doi:10.1029/2005WR003989, 2006. 8897
Sullivan, P. P., Moeng, C.-H., Stevens, B., Lenschow, D. H., and Mayor S. D.: Structure of the entrainment zone capping the convective atmospheric boundary layer, J. Atmos. Sci., 55, 3042–3064, 1998. 8897
Sykes, R. I. and Henn, D. S.: Large-eddy simulation of turbulent sheared convection, J. Atmos. Sci., 46, 1106–1118, 1989. 8897
Vinuesa, J.-F. and Porté-Agel, F.: A dynamic similarity subgrid model for chemical transformations in LES of the atmospheric boundary layer, Geophys. Res. Lett., 32, L03814, doi:10.1029/2004GL021349, 2005. 8901
Vinuesa, J.-F. and Galmarini, S.: Characterization of the ^{222}Rn family turbulent transport in the convective atmospheric boundary layer, Atmos. Chem. Phys., 7, 697–712, 2007, http://www.atmos-chem-phys.net/7/697/2007/. 8898, 8904, 8907, 8911
Yamada, T. and Mellor, G.: A simulation of the Wangara atmospheric boundary layer data, J. Atmos. Sci., 32, 2309–2329, 1975. 8901, 8902

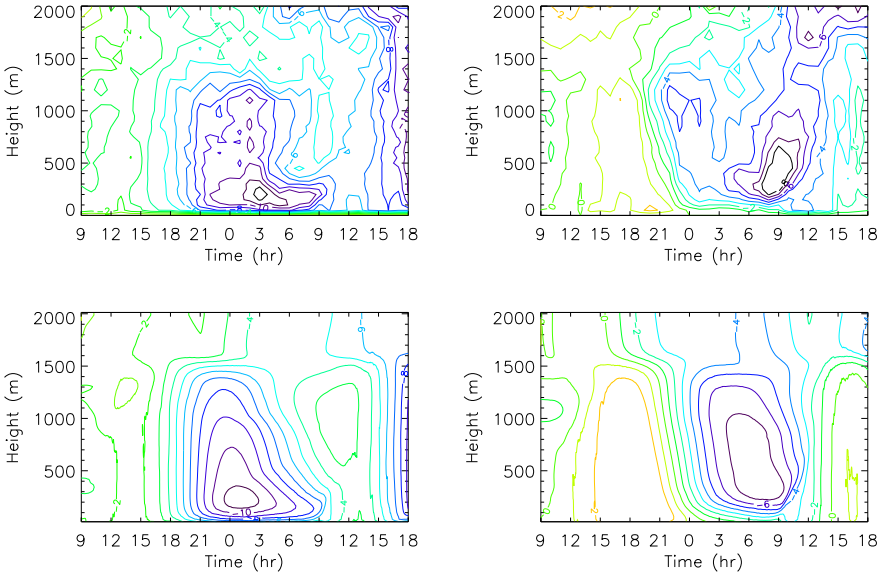

Fig. 1. Time-height plots of the observed (top) and modeled (bottom) mean longitudinal (left) and lateral (right) velocity components.

ACPD
7, 8895–8931, 2007

EGU

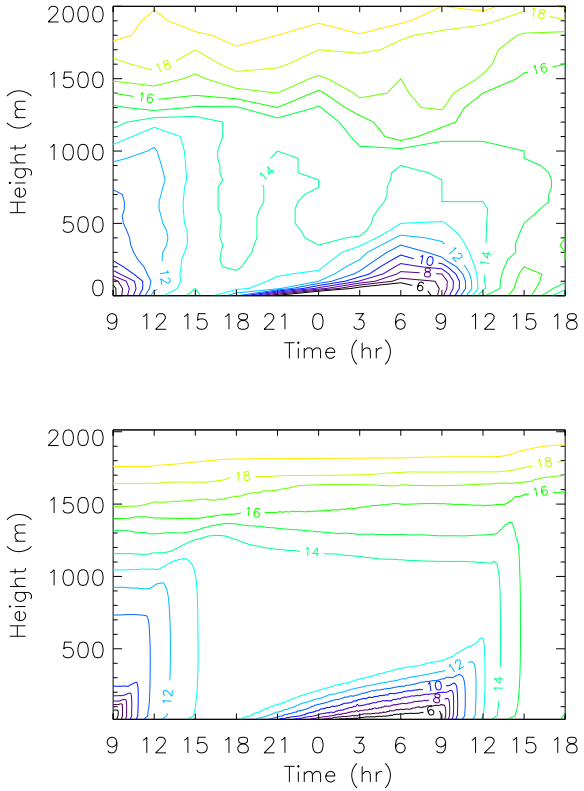

Fig. 2. Time-height plot of the observed (top) and modeled (bottom) mean potential temperature (°C).

ACPD
7, 8895–8931, 2007

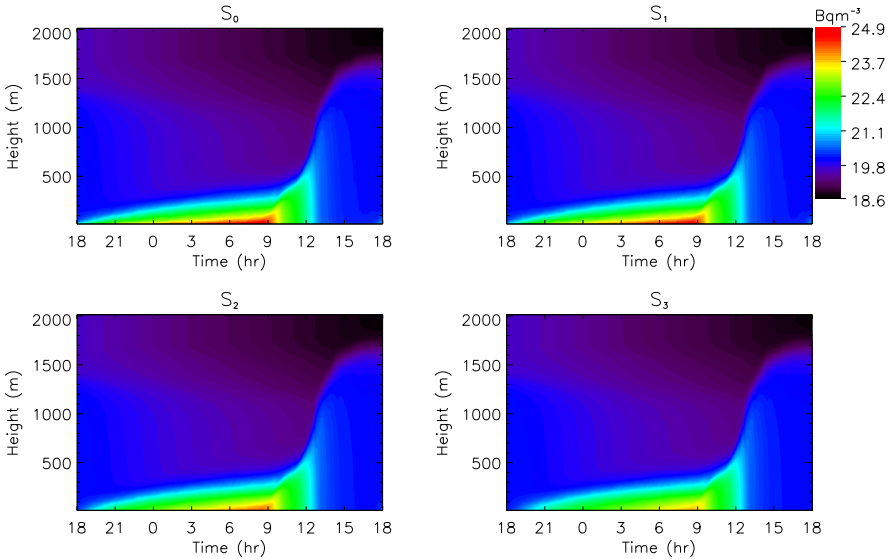

Fig. 3. Time-height plot of S_0 and its progeny.

ACPD
7, 8895–8931, 2007

EGU

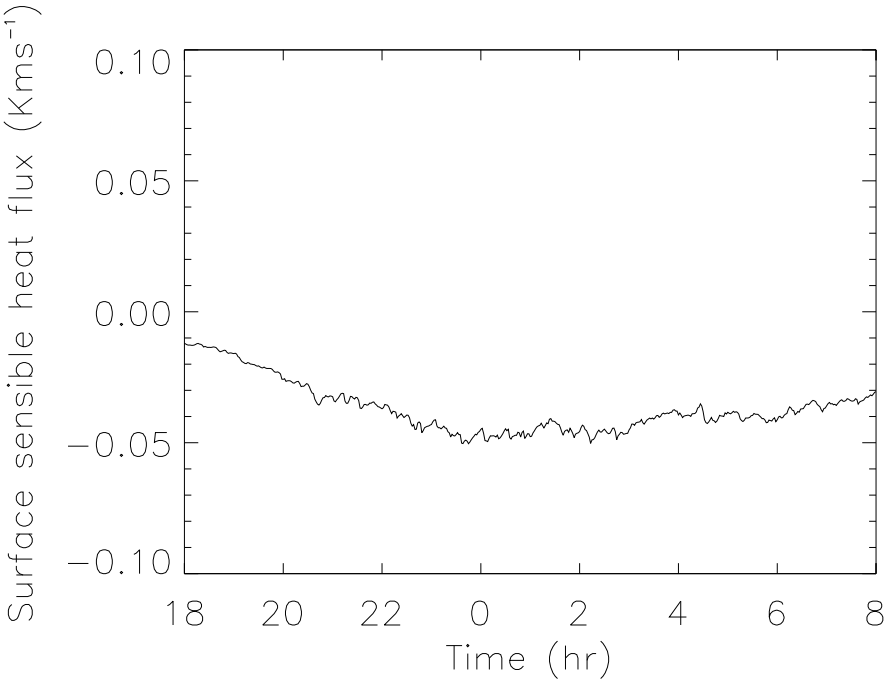

Fig. 4. Nighttime evolution of the sensible surface heat flux.

ACPD
7, 8895–8931, 2007

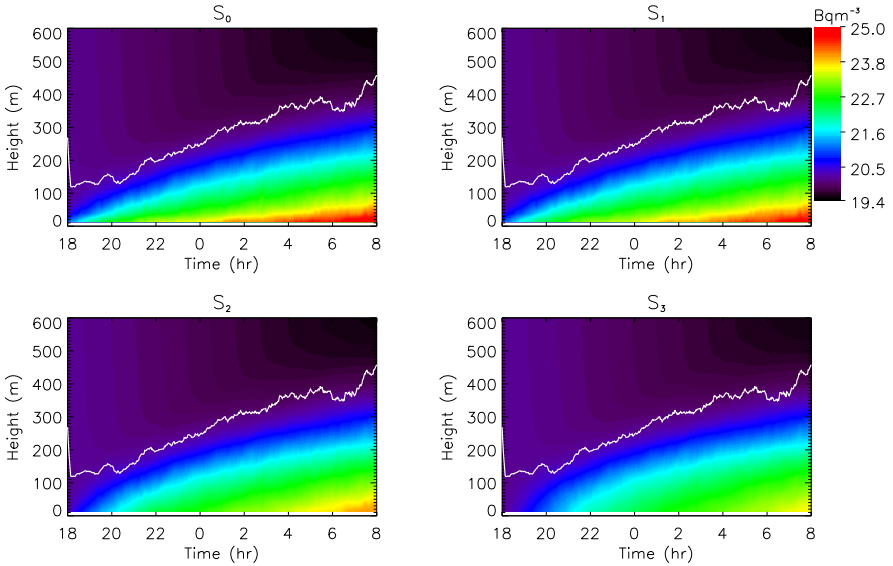

Fig. 5. Time-height plots of the radon and its short-lived daughter concentrations. The boundary layer depth is shown using a solid line. It is defined as the height where the turbulent heat flux is 5% of its surface value (Estournel and Guedalia, 1985).

ACPD
7, 8895–8931, 2007

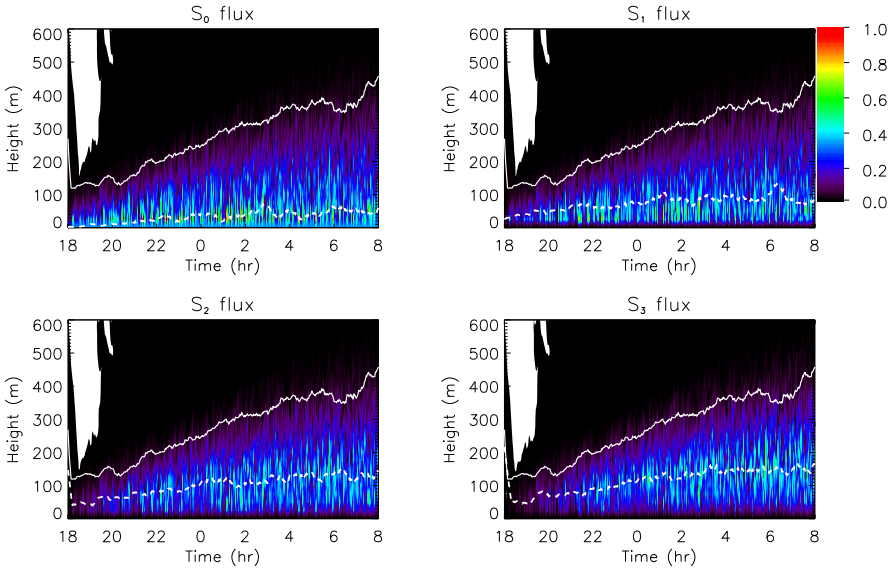

Fig. 6. Time-heightplots of the radon and its short-lived daughter dimensionless fluxes. The fluxes have been made dimensionless using their maximum values. The boundary layer depth is shown using a solid line. It is defined as the height where the turbulent heat flux is 5% of its surface value (Estournel and Guedalia, 1985). The areas in white represents downward fluxes. The localisation of the maximum fluxes is shown in dashed lines.

ACPD
7, 8895–8931, 2007

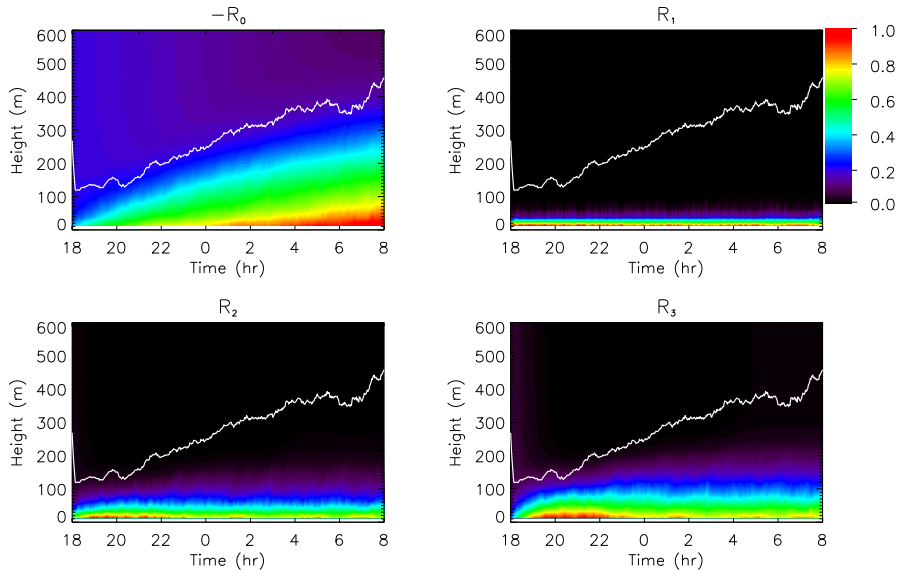

Fig. 7. Time-height plots of the radioactive decay contributions R_i. The contributions have been made dimensionless using their maximum values. The boundary layer depth is shown using a solid line. It is defined as the height where the turbulent heat flux is 5% of its surface value (Estournel and Guedalia, 1985).

ACPD
7, 8895–8931, 2007

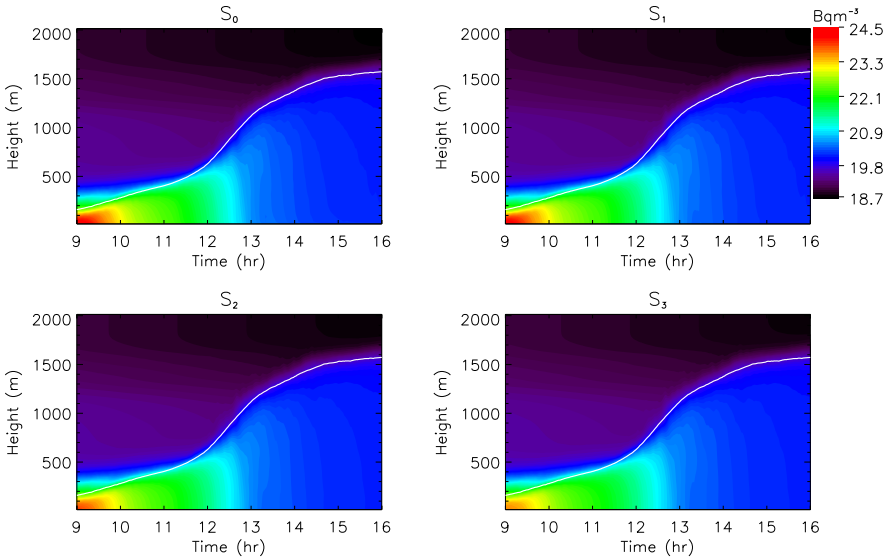

Fig. 8. Time-height plots of the radon and its short-lived daughter concentrations. The daytime boundary layer depth, defined as the altitude where the sensible heat flux is minimum, is also shown using solid white lines.

ACPD
7, 8895–8931, 2007

EGU

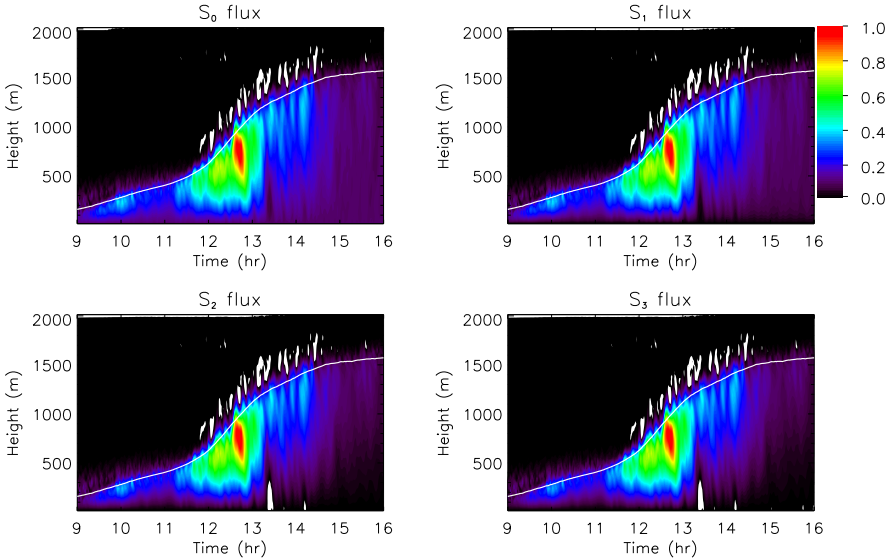

Fig. 9. Time-height plots of the radon and its short-lived daughter dimensionless fluxes.The fluxes have been made dimensionless using their maximum values. The daytime boundary layer depth, defined as the altitude where the sensible heat flux is minimum, is also shown using a solid line.

ACPD
7, 8895–8931, 2007

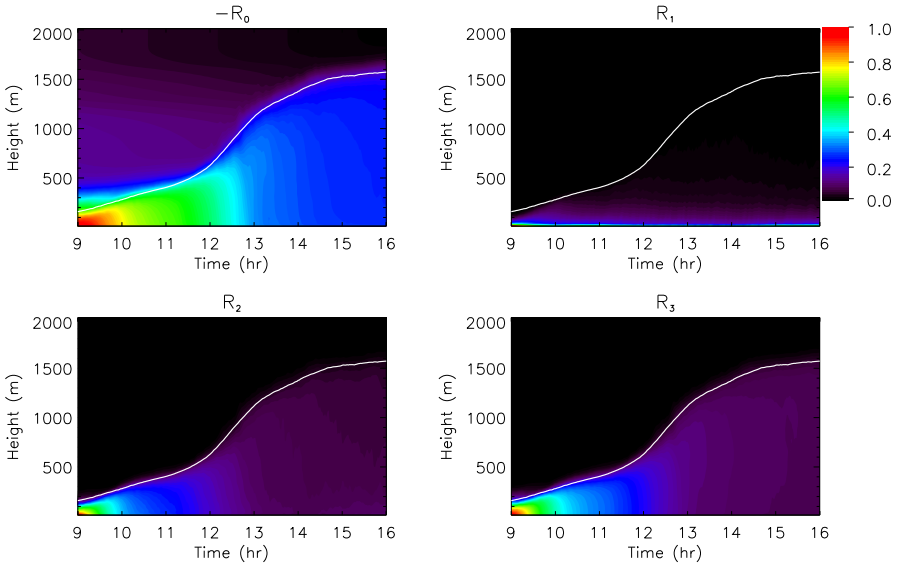

Fig. 10. Time-height plots of the radioactive decay $-R_0$, R_1, R_2 and R_3. The contributions have been made dimensionless using their maximum values. The daytime boundary layer depth, defined as the altitude where the sensible heat flux is minimum, is also shown using solid white lines.

ACPD
7, 8895–8931, 2007

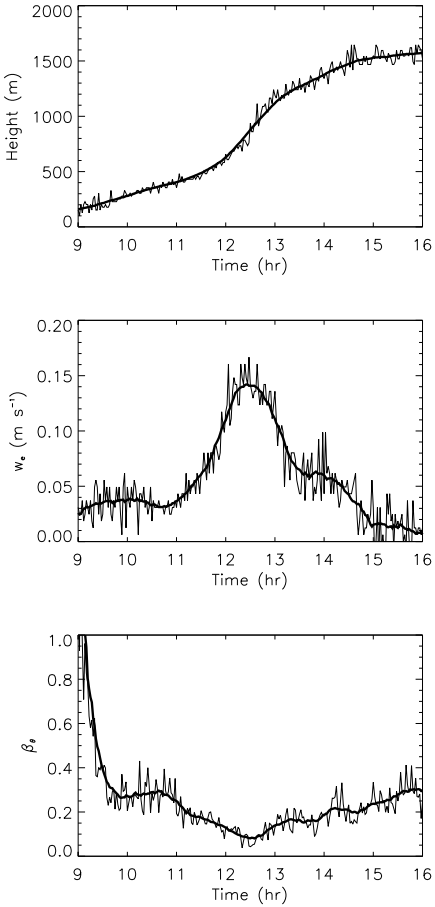

Fig. 11. Boundary layer depth z_i, entrainment velocity w_e and β_θ time evolutions. Smoothed results are also shown in thick solid lines.

ACPD
7, 8895–8931, 2007

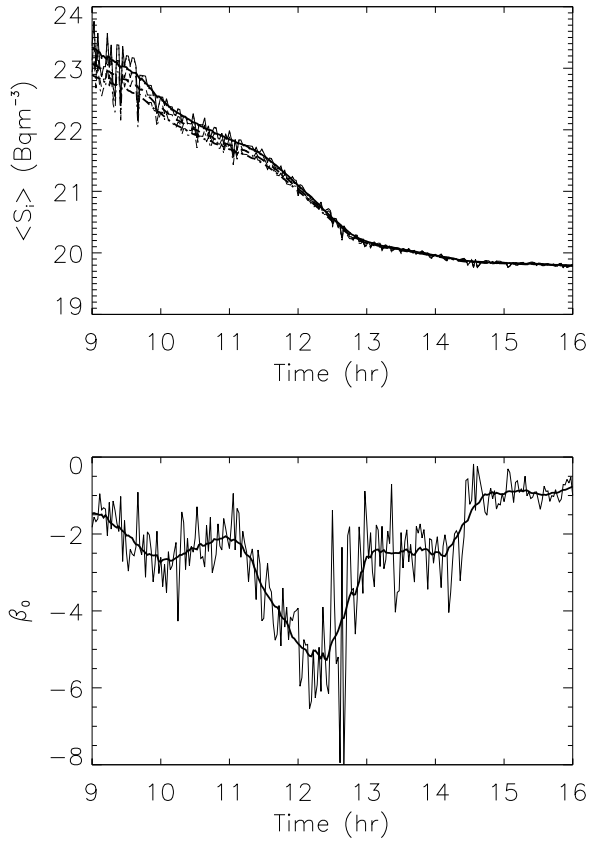

Fig. 12. Mixed layer concentrations $\langle S_i \rangle$ and β_0 time evolution. S_0, S_1, S_2, and S_3 are represented in solid, dotted, dashed and dot-dashed lines, respectively. Smoothed results are also shown in thick lines.

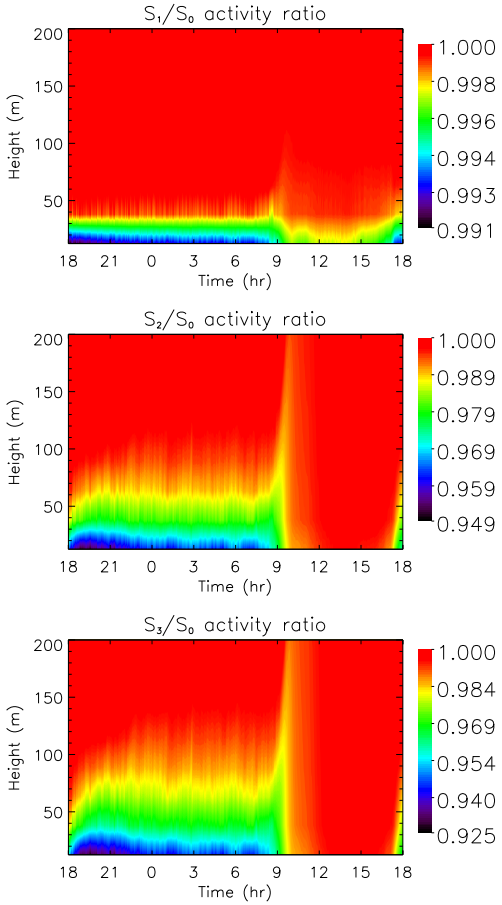

Fig. 13. Radon and its short-lived daughters activity ratio versus time-height.

ACPD
7, 8895–8931, 2007

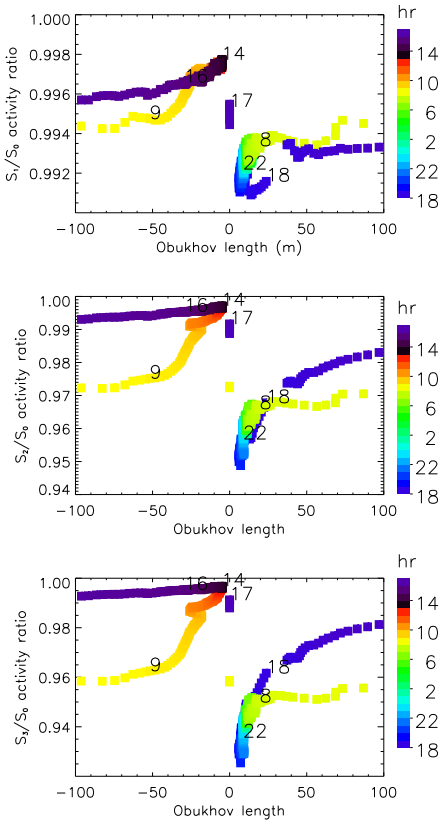

Fig. 14. Radon and its short-lived daughters activity ratio versus Obhukov length at a height of 12.5 m above ground.

ACPD
7, 8895–8931, 2007

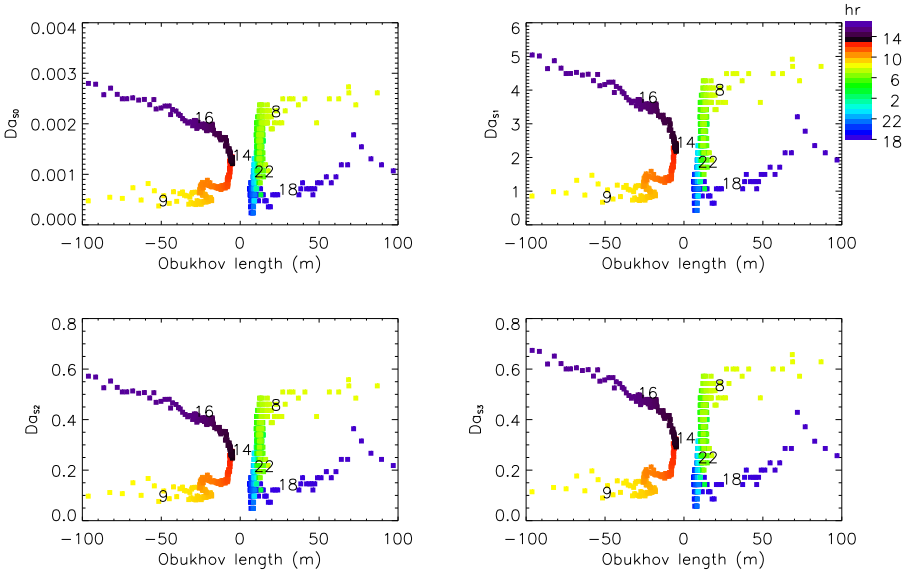

Fig. 15. Radon and its short-lived daughters Damköhler numbers versus Obhukov length.